Poly(vinylidene fluoride) Aerogels with α, β, and γ Crystalline Forms: Correlating Physicochemical Properties with Polymorphic Structures

Sruthi Suresh, Turkan Nabiyeva, Laure Biniek, E. Bhoje Gowd

Poly (Vinylidene Fluoride) Aerogels with α, β, and γ Crystalline Forms: Correlating Physicochemical Properties with Polymorphic Structures

Sruthi Suresh[†, ‡], Turkan Nabiyeva[γ], Laure Biniek[*, γ] and E. Bhoje Gowd[*, †, ‡]

[†]Materials Science and Technology Division
CSIR-National Institute for Interdisciplinary Science and Technology, Trivandrum 695 019, Kerala, India.

[‡]Academy of Scientific and Innovative Research (AcSIR), Ghaziabad 201 002, India.
[γ] Université de Strasbourg, CNRS, Institute Charles Sadron UPR22, F-67000 Strasbourg, France.

*Author for correspondence: E-mail: bhojegowd@niist.res.in
E-mail: laure.biniek@ics-cnrs.unistra.fr

Abstract

Strategic customization of crystalline forms of poly (vinylidene fluoride) (PVDF) aerogels is of great importance for a variety of applications, from energy harvesters to thermal and acoustic insulation. Here, we report sustainable strategies to prepare crystalline pure α, β, and γ forms of PVDF aerogels from their respective gels using a solvent exchange strategy with green solvents followed by a freeze-drying technique. The crucial aspect of this process was the meticulous choice of appropriate solvents to enable the formation of thermoreversible gels of PVDF by crystallization-induced gelation. Depending on the polymer-solvent interactions, the chain conformation of PVDF can be modulated to obtain gels and aerogels with specific crystalline structures. The crystalline pure α-form and piezoelectric β-form aerogels were readily obtained using cyclohexanone and γ-butyrolactone as gelation solvents. On the other hand, the γ-form aerogel was obtained using a binary solvent system consisting of dimethyl acetamide (DMAc) and water. These aerogels with distinct crystalline structures exhibit different morphologies, mechanical properties, hydrophobicity, acoustic properties, and electrical properties. Measurement of thermal conductivity for these aerogels showed exceptionally low thermal conductivity values of ~0.040 ± 0.003 $Wm^{-1}K^{-1}$ irrespective of their crystal structures. Our results showcase the fabrication approaches enabling PVDF aerogels with varied physicochemical properties for multifunctional applications.

Keywords: PVDF, thermoreversible gels, aerogels, superhydrophobic, acoustic insulation, crystalline forms

Introduction

Semicrystalline polymer-based aerogel systems are gaining wider acceptance nowadays in diverse fields such as thermal and acoustic insulation, shock-absorbing packaging materials,

oil spill clean-up, energy harvesting, electronics, etc., as they can meet all the requirements in a more comfortable way than the more fragile and brittle inorganic monoliths.[1-9] The unique ability of semicrystalline polymers to undergo thermoreversible gelation in diverse solvent environments has captured notable interest. This gelation phenomenon relies on the intricate balance between the polymer's crystalline and amorphous segments, fostering a network held together by thermally labile junction zones.[4, 10-17] These physical gels are different from the covalent gels, where the network connectivity is through crosslinking by strong covalent bonds.[18] The inclusion of crystalline domains within this gel matrix imparts remarkable robustness, resulting in distinctive attributes such as adequate porosity and mechanical strength. Several crystalline polymers are known to form thermoreversible gels and the extraction of the solvent from these gels resulted in porous polymer frameworks.[4, 11, 13-16, 19-21] Semicrystalline polymers are known to exist in a variety of crystalline forms depending on their processing conditions and polymer-solvent interactions.[22, 23] Thus in semicrystalline polymer gels, the solvents used for the gelation are expected to influence the crystal structure of the polymers. Although several semicrystalline polymers such as polyethylene,[24] isotactic polypropylene,[24] syndiotactic polystyrene (sPS),[7, 8, 11, 13, 25, 26] poly(L-lactide) (PLLA)[4, 27, 28] and PLLA/poly(D-lactide) (PDLA) blends,[4, 28] poly(ether ether ketone),[15, 29] poly(vinylidene fluoride) (PVDF),[12, 14, 16, 17, 21, 30] etc., are used for the fabrication of thermoreversible gels and aerogels, only a few studies appeared on the fabrication of aerogels having different crystalline structures. For example, the aerogels of sPS (β, γ, δ, and ε),[1, 2, 7, 8, 26, 31, 32] PPO (α and β)[33] and PLLA/PDLA blends (α and stereocomplex)[4] with crystalline forms were reported by the proper selection of gelation solvents and thermal treatments. These aerogels exhibit completely different porous morphologies and possess distinct properties and functions (e.g., thermal, dielectric, acoustic, mechanical properties, and sorption capacity of organic compounds). PVDF is a typical semicrystalline polymer with at least four distinct

crystalline forms (α, β, γ, and δ) and it exhibits unique electroactive properties (piezo-, pyro and ferroelectric).[34-43] The α form is the kinetically favored crystalline form of PVDF with a monoclinic unit cell where the polymer chains adopt trans-gauche twist (TGTG′) conformation.[37, 41, 44] The orthorhombic β form is a piezoelectric crystalline form with all-trans (TTTT) conformation.[41, 45, 46] The γ form having TTTGTTTG′ chain conformation also crystallizes into an orthorhombic unit cell and is more amorphous compared to the α and β forms.[41, 47, 48] The δ-form, which is the polar form of α form, is obtained by applying the electric field to the α form.[42, 49-52] In the case of δ-form, the two polymer chains are arrayed in parallel to the *a* axis.[38, 42, 51, 52] Great efforts have been devoted to understanding the different crystalline forms of PVDF and the pathways to obtain these crystalline forms in bulk or thin films by manipulating the processing conditions, incorporating heterogeneous phases, and tuning the polymer-solvent interactions.[34-40, 44-50] However, to date, no work has been reported on the comparison of the morphological, physicochemical and mechanical properties of PVDF crystalline aerogels and their functions.

PVDF is known to form thermoreversible gels in various solvents and attempts were made to understand the structure and gelation mechanism. Nandi and co-workers extensively studied the PVDF gelation across a spectrum of solvents and examined the morphology and crystal structures of PVDF gels prepared in various solvents.[12, 14, 16, 17, 53, 54] Maiti and coworkers investigated the thermoreversible gelation of copolymers of PVDF in phthalates with varying aliphatic chain lengths and demonstrated that the aliphatic chain length influences the gelation rate, solvent holding capability, and morphology of the gel.[55, 56] However, no attempts were made to prepare the exclusive α, β, and γ aerogels, from their thermoreversible gels, as this procedure involves gel formation and subsequent solvent extraction. The conversion of wet gels into aerogels can be achieved by extracting the gel solvent by commonly used techniques such as supercritical drying or freeze-drying. Nonetheless,

directly removing organic solvents using these methods can be challenging due to the elevated critical temperatures and pressures or the low freezing points of solvents. Consequently, it is advisable to implement solvent exchange strategies to facilitate the straightforward removal of the gel solvents. To the best of our knowledge, no reports appeared on the formation of crystal pure α, β, and γ aerogels of PVDF by this method.

Lightweight and porous PVDF materials can play a significant role in diverse fields owing to their unique properties and versatile applications. The distinctive characteristics of PVDF, combined with the advantageous features of aerogels, contribute to their multifunctional roles in various domains such as in energy harvesting, electronic fields, adsorption, catalysis, and filtration processes. The piezoelectric properties of PVDF aerogels can be utilized in flexible electronics, wearable devices, and smart textiles. Keeping these applications in mind, a few reports appeared in the literature on the creation and manipulation of PVDF aerogels and most of these focused on obtaining piezoelectric aerogels with high β fractions. Wang et al. reported the additive-free β form PVDF aerogel and used it as a triboelectric layer in a triboelectric nanogenerator.[57] Yu et al. fabricated a PVDF aerogel piezoelectric triboelectric hybrid nanogenerator by the incorporation of PANI as the conducting filler that induces more β phase content.[58] Zhang et al. fabricated PVDF aerogels with the mixture of the α and β forms by a phase inversion-induced sol-gel process and subsequent supercritical drying.[59] Torres-Rodriguez et al. attempted to prepare PVDF aerogels with adjustable morphology and phase composition by tuning the non-solvent composition in the precursor solution.[60] Recently, our group fabricated the pure β form PVDF aerogel monolith from their corresponding thermoreversible gels.[61] Although some of these reports appeared, many questions are left unanswered, particularly in understanding the structure-controlling factors in PVDF gels and aerogels. As the aerogel preparation involves solvent selection (polymer-solvent interactions), solvent exchange, and solvent evacuation, the structural changes

involved during these steps have to be clarified to obtain pure crystalline aerogels having different chain conformations (α, β and γ forms).

Herein, we proposed a simple strategy for the preparation of predominant α, β, and γ crystalline forms of PVDF aerogels using freeze-drying as the solvent extraction technique. On the basis of the thermally induced phase separation (TIPS) and nonsolvent-induced phase separation (NIPS) methods and the choice of solvents, in this study, we developed facile routes to prepare PVDF aerogels. Various organic solvents were utilized to achieve distinct crystalline forms of PVDF and these solvents were recovered fully after the solvent exchange process with ethanol and water. The pure α-form aerogel, previously unreported, was readily obtained using cyclohexanone as the gelation solvent. The predominant piezoelectric β-form aerogel was prepared using γ-butyrolactone as solvent. To achieve the γ-form aerogel, a ternary system consisting of dimethyl acetamide (DMAc) and water as solvents in combination with PVDF was employed. The aerogels with distinct crystalline structures exhibit different morphologies, mechanical properties, hydrophobicity, acoustic properties, and electrical properties. Irrespective of the crystalline form, all the aerogels demonstrated exceptionally low thermal conductivity values of ~0.040 ± 0.003 $Wm^{-1}K^{-1}$. This work provides an effective approach to fabricate PVDF aerogels with varied physicochemical properties and this approach may be extended to other semicrystalline polymers to generate aerogels with distinct properties.

Experimental Section

Materials. PVDF (average M_w ~ 534,000 g/mol by GPC, density 1.74 g/mL at 25˚C), γ-butyrolactone (ACS reagent, ≥ 99% purity), cyclohexanone (ACS reagent, ≥ 99.5% purity), and dimethyl acetate (ACS reagent, ≥ 98% purity) used in this study were obtained from

Sigma-Aldrich Co. All of the above chemicals were used as such without further purification. Distilled ethanol and Millipore water were used for solvent exchange.

Preparation of the *α* and *β* Form Aerogels of PVDF.

The *α* and *β* form aerogels of PVDF were fabricated by a two-step procedure involving thermoreversible gelation and freeze-drying. The *α* and *β* form aerogels were obtained from the gels of PVDF in cyclohexanone and *γ*-butyrolactone, respectively. Briefly, a certain amount of PVDF was dissolved in these solvents at a temperature close to their boiling points. The homogeneous solutions with a polymer concentration of 10 wt% obtained in both the solvents were then transferred into polypropylene vials under ambient conditions and cooled down to room temperature slowly to obtain thermoreversible gels. In this process, thermally-induced phase separation (TIPS) happens during cooling to obtain thermoreversible gels. Such obtained gels were aged at room temperature for 2 h, and by immersing in ethanol and ethanol/water mixtures the gel solvent was exchanged systematically as reported in our previous work.[26] Initially, the gels of PVDF were fully dipped in ethanol to replace the existing gel solvent (*γ*-butyrolactone or cyclohexanone), and then the solvents were decanted. Next, the gels were repeatedly rinsed with a mixture of ethanol/distilled water (50/50 vol/vol). Finally, the gels were kept in water for 1 h to obtain hydrogels. The entire solvent exchange process was carried out for 12 h. These hydrogels were transferred to a freezer (at - 60 °C) and kept at - 60 °C for 12 h and then lyophilized to obtain aerogels with ~ 90% porosity. The gel solvents were recovered after the solvent exchange process using a rotary evaporator.

Preparation of the *γ* Form Aerogel of PVDF.

The *γ* form aerogel of PVDF was procured by following the nonsolvent-induced phase separation (NIPS) procedure. To prepare the *γ* gel of PVDF, a combination of dimethyl acetamide (solvent) and water (nonsolvent) was used. PVDF powder was first dissolved

completely in dimethyl acetamide by heating at 90 °C, subsequently, water was slowly added into the polymer solution with stirring (dimethyl acetamide/water, 4:1 (v/v)). Then the final solution was transferred into a plastic mold kept at room temperature to obtain gel through the NIPS process. Such obtained γ form gel was aged for 2 h at room temperature and subjected to a solvent exchange process followed by freeze-drying as described in the earlier section. In the final solution, the polymer concentration was 10 wt %.

We prepared varieties of α, β, and γ aerogel samples, each with distinct shapes and dimensions, to facilitate various characterizations.

Characterization

The apparent density of various aerogel samples was determined theoretically from their mass/volume ratio. Then the porosity was determined from the density values using the following equation,

$$\text{Porosity: } 100\left[1-\frac{\rho_{ap}}{\rho_{pol}}\right]$$

where ρ_{ap} is the mass/volume ratio (apparent density) of the prepared aerogel, the volume is determined theoretically from the dimensions of the samples, and ρ_{pol} is the density of the bulk polymer. The crystal structures of α, β, and γ gels, hydrogels, and aerogels were analyzed using Wide-Angle X-ray Diffraction (WAXD) patterns obtained from the XEUSS SAXS/WAXS system from Xenocs. This system employed Cu Kα radiation with a wavelength (λ) of 1.54 Å in transmission mode, and data were collected using a Mar 345 image plate detector. Data processing of the 2D-WAXD patterns was performed using the Fit2D software. Variable temperature WAXD measurements were conducted with a Linkam THMS 600 hot stage connected to the LNP 95 cooling system. Gels and hydrogel samples were taken in a capillary tube and placed in a sample holder for analysis and aerogel samples were sliced using a surgical blade and placed directly in the X-ray path. The microstructures were further characterized through Fourier Transform Infrared spectroscopy (FTIR) using

PerkinElmer's Spectrum Two FTIR spectrometers. FTIR/ATR spectra were acquired under atmospheric conditions, involving 32 scans with a resolution of 4 cm^{-1}. For ATR analysis, a small portion of the pre-dried aerogel sample was directly placed on a sample holder and the spectrum was obtained at different regions. To examine the morphologies of the three aerogels, scanning electron microscopy (SEM) was employed. SEM measurements were carried out using a Zeiss EVO 18 cryo-SEM operating at an accelerating voltage of 20 kV. The wetting behavior of the aerogels was assessed by measuring water contact angles (WCA) at room temperature. This was achieved using an automated DSA30 Drop Shape Analyzer by KRŰSS in Germany. The thermal stability and degradation behavior of all aerogels were monitored using a thermogravimetric analyzer (TGA) TA Q50. The samples were heated from room temperature to 800 °C at a rate of 10 °C/min under a nitrogen atmosphere. Differential Scanning Calorimetry (DSC) measurements were performed using an advanced research-grade modulated differential scanning calorimeter TA Q2000 under a nitrogen gas flow. Samples were heated from room temperature to 200 °C at a rate of 10 °C/min and then cooled back to room temperature at the same rate. Compression tests were conducted on cylindrical aerogel samples to evaluate their mechanical performance. A Universal Testing Machine (Hounsfield, H5KS UTM, Redhill, UK) with a crosshead speed of 1.5 mm/min was used for these tests. The thermal conductivity of the aerogels was measured using the transient plane source (TPS) technique with a commercial apparatus (Hot Disk®, TPS 1000). The method, optimized for bulk size and low thermally conducting samples, was detailed in a previous work.[62] The experiments were performed in ambient conditions and at room temperature. The input power and time duration were set at 5 mW and 40 s, respectively. The measurements were repeated four to five times, with 45 min stabilization between each measurement. In this method, a sensor with a radius of 3.189 mm, composed of a Nickel double spiral protected with a thin layer of Kapton insulator, was placed between two PVDF

aerogels. The normal incident sound absorption coefficient of all the samples was determined using a Brüel and Kjær impedance tube, type 4206 (Denmark), via the two-microphone method. Cylindrical samples with a diameter of 29 mm and a thickness of 12 mm were used for these measurements.

Results and Discussion

Tazaki et al. conducted an insightful study focusing on the thermoreversible gelation behavior of PVDF in various aliphatic and cyclic ketones.[30] This research sheds light on the intricate interplay between PVDF and different solvent environments, providing valuable insights into the gelation phenomenon. In this work, we successfully prepared α and β form PVDF aerogels from PVDF gels in cyclohexanone and γ-butyrolactone, respectively, using the TIPS method and the γ form PVDF aerogel from PVDF gel in DMAc/water using the NIPS method as illustrated in **Figure 1**. The polymer concentration in the solution was kept at 10 wt% in all three cases. The thermal and mechanical properties of PVDF gels were not discussed in this work, as these properties are sensitive not only to the crystalline forms but also to the concentration of the polymer and the polarity of the gel solvent. It was reported that the PVDF crystalline forms are affected sensitively by the nature of the solvent used and also by the crystallization conditions (temperature and crystallization rate).[63, 64] As detailed in the Experimental Section, the gelation solvent was exchanged with ethanol and water before freeze-drying to obtain the respective aerogels.

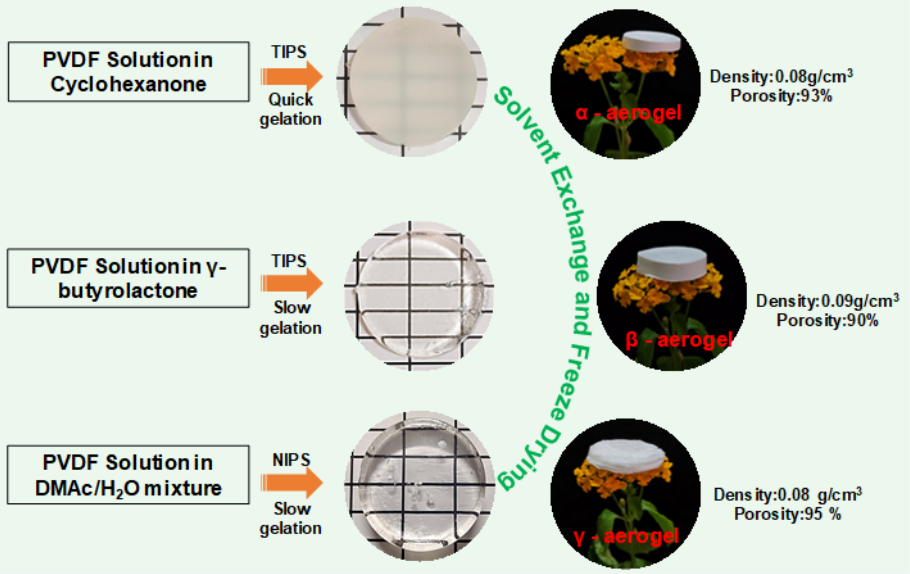

Figure 1. Schematics showing the synthesis procedures of α, β, and γ aerogels of PVDF.

Thermoreversible Gelation of PVDF in Cyclohexanone and the α Form Aerogels

PVDF gel in cyclohexanone was prepared by cooling the solution to room temperature. As already reported, in semicrystalline polymers, the gel is formed from a polymer solution due to a liquid−liquid phase separation followed by the formation of crystalline domains in the polymer-rich phase.[29, 65] The crystallization-induced phase separation occurred rapidly during the cooling of PVDF/cyclohexanone solution and the wide-angle X-ray diffraction pattern shows the peaks at 2θ = 17.8° (100), 18.3° (020), 20.0° (110) and 26.7° (021) corresponding to the typical α form of the PVDF (**Figure 2a**, top panel).[41] The gel solvent, cyclohexanone was exchanged with a higher freezing temperature (0 °C) solvent, water. No major change in the physical appearance of the gel was observed during the solvent exchange process and WAXD peak positions remain almost the same indicating that the α form structure was retained (**Figure 2a**, middle panel). The variation in the peak intensities and full width at half maximum (FWHM) indicates that the PVDF further crystallized into the α form during the solvent exchange process. Subsequently, following a systematic solvent exchange process, the gel was freeze-dried to obtain the α form aerogel (**Figure 2a**, bottom panel). The FTIR

spectrum of the aerogel showed the IR bands corresponding to the α form at 976 cm^{-1} and 1210 cm^{-1} (**Figure 2d**, top panel).[66] The resultant α form aerogel is visually depicted in **Figure 1** because it's incredibly lightweight, the aerogel can rest gently on top of the flower without causing any noticeable weight.

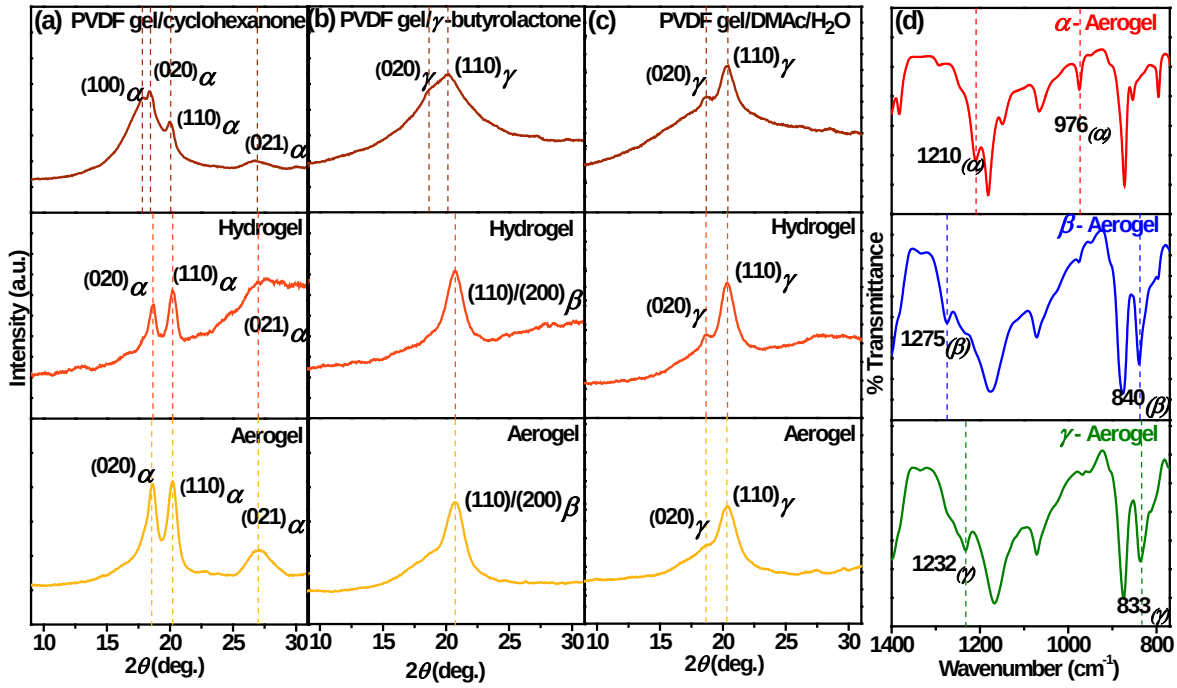

Figure 2. WAXD patterns of PVDF gel, hydrogel (after solvent exchange) and aerogel prepared using different solvents (a) cyclohexanone, (b) γ-butyrolactone, and (c) DMAc/ Water system, and (d) FTIR spectra of α, β, and γ aerogels.

Thermoreversible Gelation of PVDF in γ-butyrolactone and the β Form Aerogels

In order to obtain the β form aerogel, γ-butyrolactone was chosen as a gel solvent for PVDF. As described in the literature, γ-butyrolactone (with a Flory-Huggins interaction parameter, $\chi_{12} = 0.5$) is a relatively more favorable solvent for PVDF compared to that of cyclohexanone (where $\chi_{12} > 0.5$).[67] This disparity in polymer-solvent interactions influenced our observations during gelation. The gelation process exhibited faster kinetics in cyclohexanone compared to γ-butyrolactone. Since the thermodynamics of gelation of PVDF in cyclohexanone (χ12>

0.5), and γ-butyrolactone ($\chi 12 = 0.5$) are different, the gelation kinetics and thermodynamics determine the crystal structures of PVDF in these solvents. **Figure 1** illustrates a distinct contrast between the two gels produced. The gel derived from γ-butyrolactone showcases a remarkable transparent nature, while the one originating from cyclohexanone presents an opaque appearance. This visual dissimilarity further underscores the divergent gelation dynamics and possibly hints at variations in their microstructures. After the solvent exchange process, the PVDF/γ-butyrolactone gel undergoes a complete transition from a transparent to an opaque state. The WAXD pattern of the PVDF/γ-butyrolactone gel shows peaks corresponding to the disordered γ form at $2\theta = 18.4°$ (020) and 20.2° (021) (**Figure 2b**, top panel).[41] Fischlschweiger and co-workers reported the formation of the γ form of PVDF using γ-butyrolactone and they demonstrated that the crystallization temperature of the PVDF solution determines the fractions of the α and γ forms. In the present work, PVDF gel in γ-butyrolactone shows the predominant γ form.[64] However, unlike PVDF/cyclohexanone gel, PVDF/γ-butyrolactone gel shows a crystal-crystal transition upon the solvent exchange process and the γ form is transformed to the β form, $2\theta = 20.7°$ (110/200) (**Figure 2b**, middle panel).[41, 44] To enhance our understanding of this crystal-crystal transition, we measured WAXD patterns upon the systematic exchange at different time intervals (Figure S1). Initially, the WAXD peak corresponding to the (021) diffraction planes of the disordered γ form was centered around 20.2°. Subsequent to the addition of ethanol to the gel, there was an immediate shift in the peak to 20.7° (110/200), arranging to a more polar β form. Here, even after achieving stable gel, the amorphous PVDF chains persist in a mobile state. Consequently, during the solvent exchange process, when these chains come into contact with a non-solvent, it can trigger a reorganization of the crystal structure. Upon the solvent extraction using a freeze-drying process, a stable β form aerogel was obtained as evident by the WAXD pattern ($2\theta = 20.7°$ (110/200)) (**Figure 2b**, bottom panel) and FTIR spectrum

(**Figure 2d**, middle panel). A strong dominant FTIR peak at 1275 cm^{-1} readily confirms the formation of β form aerogel.[66]

Thermoreversible Gelation of PVDF in DMAc/Water System and the γ Form Aerogels

Ternary mixtures of a polymer with a solvent and a nonsolvent are widely used primarily for the preparation of membranes by nonsolvent-induced phase separation (NIPS). Ternary phase diagram for PVDF/DMAc/water system has been extensively studied in the case of membranes and these are well established.[68] However, investigations into aerogels, as well as their studies pertaining to crystalline characteristics and morphologies, have not been conducted within this system. The introduction of even a small amount of water can trigger the crystallization of PVDF into alternative forms. Nevertheless, managing the polymer chain conformation and achieving the desired crystalline forms remains a considerable challenge. In this work, a combination of DMAc and water in a 4:1 ratio was utilized to successfully produce the γ form aerogel. Following the dissolution of PVDF in the DMAc, water was added slowly to the polymer solution. The resulting gel was then left undisturbed for some time to establish stability and it appears transparent as seen in **Figure 1**. The WAXD pattern of this gel shows peaks at 2θ = 18.4° (020) and 20.2° (110), corresponding to the γ form of PVDF (**Figure 2c**, top panel).[41] Tashiro et al. prepared the as-cast film of PVDF from DMAc solution and assigned the obtained crystalline form to the disordered γ form (as-cast form III) based on the presence of infrared bands at 840 and 1275 cm^{-1}.[69] Unfortunately, the infrared spectrum of the gel shows the saturated bands of the DMAc rendering the infrared bands assignment difficult. Based on the published literature, the γ form obtained from the solution crystallization was assigned as the disordered γ form.[69] Subsequently, a solvent exchange technique was applied to achieve a stable gel and the WAXD pattern remains the same with a slight increase in their intensities indicating that the disordered γ form is retained after the solvent exchange process (**Figure 2c**, middle panel). Upon the solvent extraction by freeze-

drying resulted in the pure γ form aerogel (**Figure 2c**, bottom panel). The crystalline purity was further confirmed by FTIR and the aerogel shows bands at 833 cm^{-1} and 1232 cm^{-1}, corresponding to the pure γ form aerogel (**Figure 2d**, bottom panel).[66] The FTIR spectrum of aerogel (shows IR bands at 1232 cm^{-1} and 833 cm^{-1}) matches well with the high-temperature annealed spectrum of the γ form (Form III) as reported by Tashiro et al.[69]

As discussed in the preceding sections, the sequential solvent exchange step involving ethanol followed by water, i.e., converting gels into hydrogels, is crucial as it enables the avoidance of structural distortions that typically arise during the freeze-drying of gels. Moreover, it contributes to the overall environmentally friendly nature of the processing pathway by facilitating the reclamation of organic solvents by distillation, rendering them suitable for subsequent reuse. We could achieve PVDF aerogels with porosities as high as 90%, and there was only negligible shrinkage to the gel structures upon freeze-drying.

Morphology and Surface Properties of α, β and γ Form Aerogels

As seen in the preceding section, the gelation process is mainly dictated by polymer crystallization, and the gelation solvent influences the crystalline phase of PVDF, the obtained aerogels are expected to show different morphological features. **Figure 3** illustrates the surface morphologies of the three different aerogel specimens at varying magnifications. All three of them exhibit entirely distinct morphologies in their appearances. The α form aerogel reveals the highly interconnected open porous network structures consisting of fibrillar morphology (**Figure 3a**). The fiber diameters are relatively small, measuring around 300 nm. Cyclohexanone is a relatively poor solvent for PVDF and the polymer chains crystallize rapidly into nanofibrous structures. These nanofibrous structures bundle by connecting with each other to form the gel network. The gel morphology is retained during the solvent exchange and solvent extraction processes. The α form aerogels have resulted in

hydrophobic surfaces with a water contact angle of ~ 132°. On the other hand, the β form aerogel obtained from PVDF/ γ-butyrolactone gel shows highly interconnected denser spherulitic structures having dimensions ranging from 4 to 6 μm (**Figure 3b**). As seen in Figure 1, the PVDF/γ-butyrolactone gel appears transparent and it was reported that in transparent gels larger spherulites do not exist. Tazaki et al. reported that spherulites were not observed in the slowly cooled gel and the morphology of the gel was strongly influenced by the cooling rate of the hot PVDF solution.[30] The Flory-Huggins interaction parameter is inversely proportional to the temperature and the cooling rate of the hot solution influences the polymer-solvent interactions strongly.[67] As a result, the cooling rate of the solution may significantly influence the spherulite dimensions as well as the transparency of the gel. As discussed in the preceding section, a major structural reorganization took place from the disordered γ form to the β form during the solvent exchange process. Based on this, we speculate that the solvent exchange process is responsible for the spherulitic morphology in the β form aerogel. It has to be noted that the Flory-Huggins interaction parameter of PVDF in γ-butyrolactone is smaller than cyclohexanone and the γ-butyrolactone is a relatively good solvent for PVDF compared to cyclohexanone.[67] Due to this reason, the gels and aerogels obtained using these solvents exhibit different morphologies. In addition, nodule-like structures were observed on the surface of the spherulites in a magnified SEM image of the β form aerogel. Due to this, a significant increase in the water contact angle was observed in the case of β form aerogel. The water contact angle raised to 148° in the β form aerogel rendering them superhydrophobic materials.

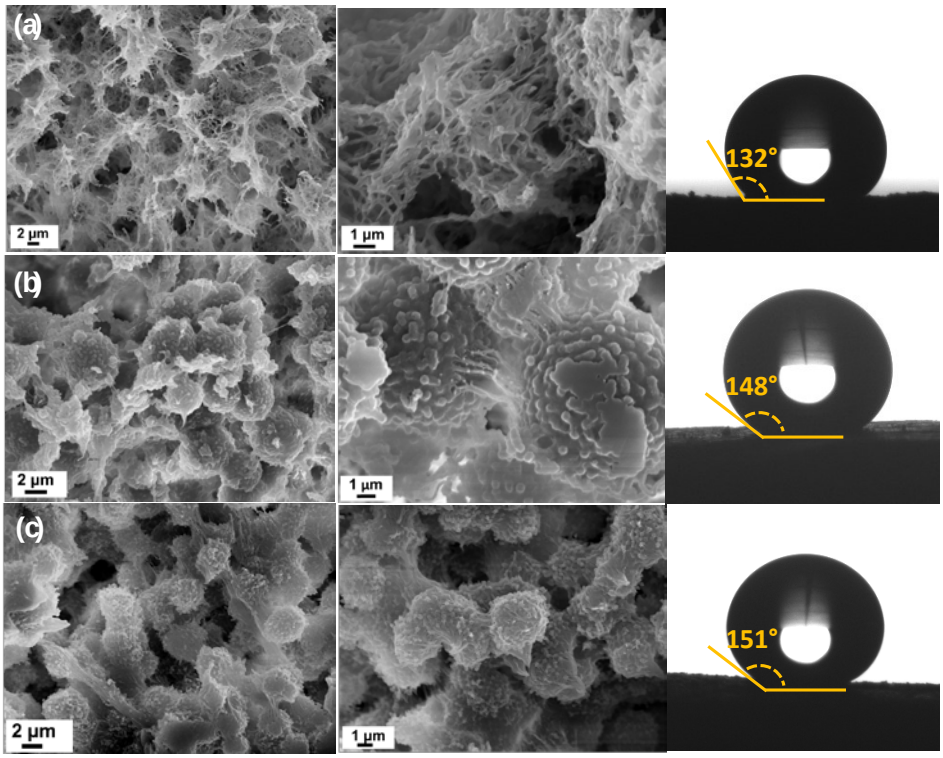

Figure 3. SEM images and water contact angles for (a) α form, (b) β form, and (c) γ form aerogels.

The disordered γ form aerogel also exhibited a spherulitic morphology adorned with minuscule pearl-like features on its surface (**Figure 3c**). The spherulites exhibit greater continuity with well-established interconnections. Unlike the α and β form aerogels, the presence of the nonsolvent in DMAc/water plays a crucial role in the gel formation and the nonsolvent dictates the morphology of the PVDF gel and aerogel. In contrast to the β form aerogel, the dimensions of these spherulites are smaller (2 to 3 μm) and the spherulitic structures in this instance exhibit a degree of porosity due to the loose winding of the polymer fibrils. The porosity along with the minuscule globules residing on the surface of the γ form aerogel further enhances the surface properties. The water contact angle further increased to 151° in the case of the γ aerogel and the surface exhibited the phenomenon of water droplets rolling off. The water droplets rapidly rolled out from the surface of the γ aerogel, showing very low adhesion to the water (Movie S1). These findings align with the Cassie-Baxter

wetting model, which anticipates that on a rough hydrophobic surface, a nonwetting liquid may not infiltrate surface cavities.[70, 71] This leads to the creation of air pockets and the establishment of a composite solid-liquid-air interface, consequently enhancing hydrophobicity.

Mechanical, Thermal and Electrical Properties of *α*, *β* and *γ* Aerogels

Mechanical stability is one of the key parameters for the applications of aerogels and the mechanical performance of *α*, *β* and *γ* aerogels (porosity ~ 90%) were examined by compression tests and the corresponding stress−strain curves are shown in **Figure 4a**. All the aerogels displayed typical stress-strain behavior characteristic of open-cell porous materials. The compression moduli and Young's moduli measured from the stress−strain curves are summarized in **Table 1** for various aerogels. The aerogels exhibited a linear increase initially, signifying the elastic region, followed by a nonlinear plastic-yielding plateau in the intermediate region, which corresponds to the deformation of the pore structure. At higher limits, with the increase in stress, aerogels displayed an irreversible buckling behavior and underwent a transformation into dense solids, similar to other semicrystalline polymer-based aerogels.[4, 6] Nevertheless, the compressive modulus, as calculated from the slope of the linear elastic region of the stress-strain curve, was notably lower for the *γ* aerogel (~ 0.64 MPa), in contrast to the *α* (~2.17 MPa) and *β* aerogels (~3.49 MPa). When subjected to a 40% strain, the *β* aerogels exhibited a maximum stress value of ~1.47 MPa, which serves as a clear indicator of their superior load-bearing capacity in comparison to other semicrystalline aerogels. These results clarified that the variance in compressive modulus primarily arises from disparities in the structure and morphology of the aerogels, as discussed in the preceding sections. Further, as depicted in **Figure 4b**, *α* and *β* aerogels demonstrate the remarkable ability to withstand a load nearly 2000 times their own weight without undergoing structural disintegration. However, with comparable porosity, the *γ* aerogel

supports a load that is 1000 times its initial weight. These results clarified that the β form aerogel exhibits better mechanical performance among the piezoelectric phases (β and γ).

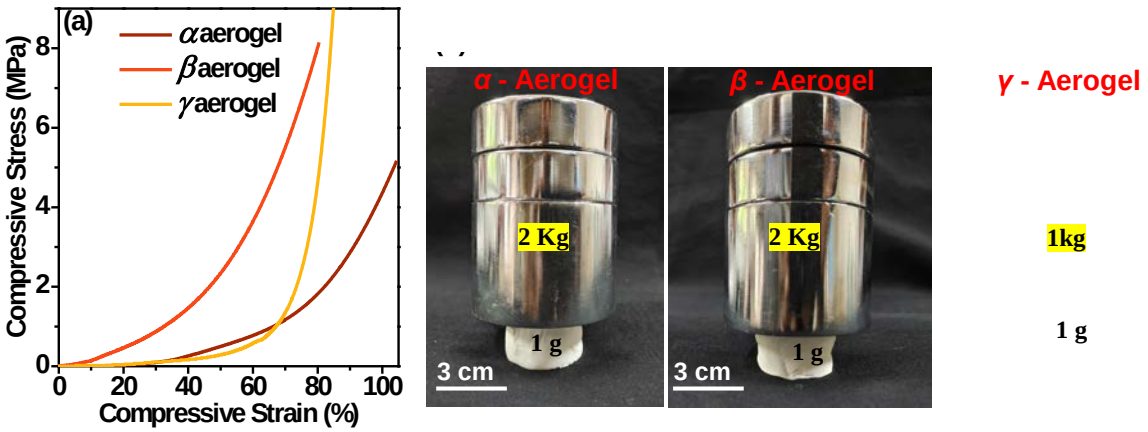

Figure 4. (a) Compressive curves and (b) photographs depicting load bearing capacity of α, β and γ form aerogels.

The thermal stability of aerogels holds greater significance for their practical applications and processing requirements, as they can be influenced by the preparation conditions. **Figure 5a** depicts the TGA thermograms of α, β and γ form aerogels and each of these crystalline forms exhibited a similar degradation trend albeit a slight variation in the onset of degradation and char residues. The preparation methods adopted to obtain different polymorphic aerogels using different solvents might have influenced the degradation behavior of various aerogels. Table 1 summarizes the onset of degradation and 50% weight loss for α, β and γ form aerogels. Each of the acquired forms exhibited thermal stability of ~ 370°C, rendering them suitable for use in applications requiring higher operational temperatures. The decomposition of the polymer chain backbone as evident from the major weight loss occurred in a broad temperature range of 370 to 470 °C. DSC thermograms of these aerogels (**Figure S2**) showed a single broad melting peak in the temperature range of 155-160 °C. The degree of

crystallinity (ϕ_{DSC}) estimated for various aerogels from the enthalpy of melting endotherms (ΔH_m) by,

$$\phi_{DSC} = \frac{\Delta H_m}{\Delta H_{100}}$$

(where ΔH_{100} = 104.7 J/g is the enthalpy of 100% crystallized PVDF)[72] and the crystallinity values are summarized in Table 1. These values are higher than the degree of crystallinity measured from the WAXD patterns of aerogels by taking the ratio of area under the crystalline peaks to the total area.

Table 1. Summary of mechanical and thermal properties of *α*, *β* and *γ* form aerogels.

Sample	**Young's Modulus (MPa)**	**Compression Stress @ 40% Strain (MPa)**	**T_{10} (°C) (±1)**	**T_{50} (°C) (±1)**	**T_m (°C) (± 0.3)**	**% Crystallinity of Aerogels (± 0.5)**	
						WAXD	**DSC**
α-Aerogel	2.17	0.26	395	444	158	50	51
β-Aerogel	3.49	1.47	405	440	157	42	45
γ-Aerogel	0.64	0.16	428	448	157	40	49

PVDF is widely used as a piezoelectric material and the piezoelectric performance mainly depends upon the crystalline form of the polymer. The thermodynamically stable *α* form adopts TGTG′ chain conformation and two of these chains are packed in the monoclinic unit cell and are connected by a point of symmetry. The CF_2 dipoles' orientation directions are opposite to each other and as a result, this crystalline form is nonpolar.[37, 41, 44] The chain conformation of the *β* form is all trans (TTTT)-zigzag type and these chains are packed in the orthorhombic unit cell with their dipoles parallel to the *b* axis. This is a polar crystalline form and it is a ferroelectric crystal.[45, 73, 74] The *γ* form chains take TTTGTTTG′ conformation and these chains are packed in parallel along the *a* axis to offer the polar crystal. It was reported

that these chain conformations are sensitive to external stimuli such as temperature, electric field, mechanical force, and so on resulting in structural changes.[39, 47] Herein we verified the stability of these crystalline forms by conducting the variable temperature WAXD measurements during the heating process at an interval of 10°C for α, β and γ form aerogels as depicted in **Figure 5b-d**. As seen, all three crystalline forms (α, β and γ) remain stable up to their melting temperatures. These results clarified that the chain conformation and the dipole alignments remain the same in the heating process up to their melting and hence suitable for high-temperature applications.

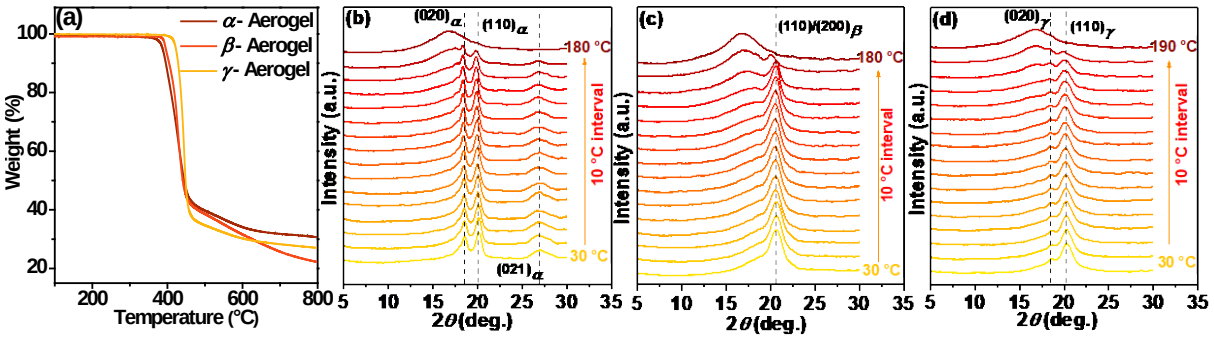

Figure 5. (a) TGA thermograms and (b-d) temperature-dependant WAXD patterns of α, β and γ aerogels in the heating process (WAXD patterns were collected at an interval of 10 °C).

To be engaged in ferroelectric devices, a ferroelectric crystal needs to exhibit remnant polarization and a low coercive field. As discussed in the preceding section, β and γ forms are electrically active crystalline forms and their piezoelectric effect depends on net dipole density and the alignment of dipoles. To verify the ferroelectric properties of β and γ forms, ferroelectric behavior was studied by polarization-electric field (P-E) hysteresis loop tests at room temperature and the results are shown in **Figure 6**. The measurements were carried out using 1 cm^2 aerogel samples at 10 Hz in an applied voltage sweep ranging from -0.8 kV to 0.8 kV. Both the aerogels demonstrated non-linear polarization behavior and the β form aerogel exhibited a higher remnant polarization (0.02 $\mu C/cm^2$) and a coercive field of 0.27

kV/cm than that of the γ form aerogel (remnant polarization: 2.47x 10^{-5} μC/cm^2 and coercive field of 0.20 kV/cm). These results suggest that a higher number of ferroelectric crystalline domains exist in the β form aerogel and it enables more effective dipole alignment when subjected to an applied electric field than the γ form aerogel. However, the nonpolar α form exhibited a very weak P-E loop in the applied electric field. The complete saturation in the hysteresis cycle is not achieved because of the instrument's limitation to apply higher voltages.

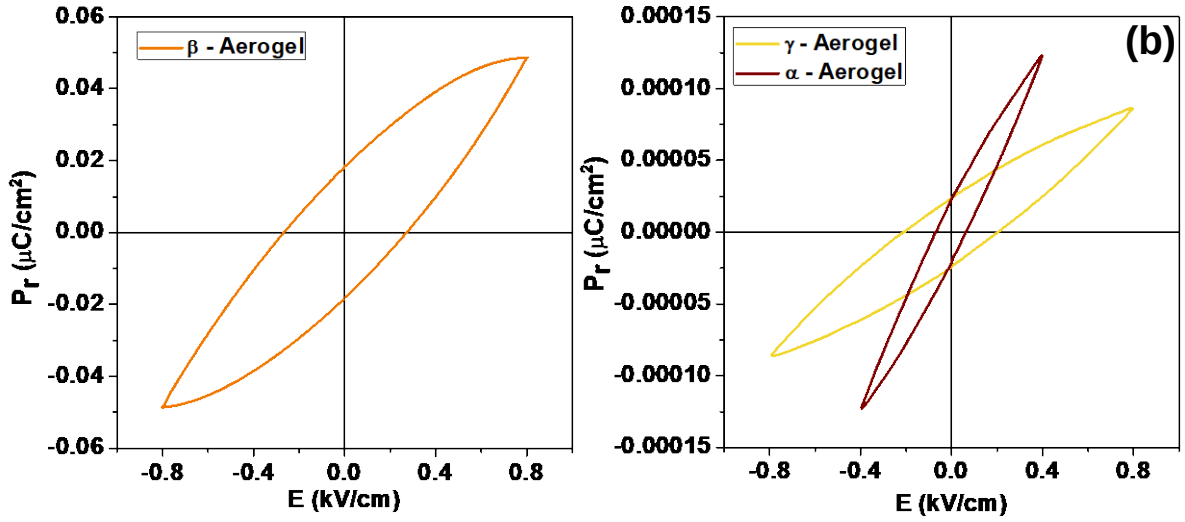

Figure 6. P- E hysteresis loop analysis of (a) β and (b) γ and α aerogels.

Thermal Conductivity and Acoustic Properties of *α*, *β*, and *γ* aerogels

Aerogels have a large potential to excel as thermal insulation materials due to their porosity with diverse network structures. The experimental reports have been quite limited in understanding the influence of the crystal structure of the polymer aerogels on thermal conductivity. Further, there has been limited exploration into the thermal conductivity performance of PVDF aerogels and its dependence on morphology. Generally, heat transfer within aerogels occurs through solid conduction, gaseous conduction, and radiative transmission. The combination of these three components determines the overall thermal

conductivity (λ) of the aerogel. The thermal conductivity of the PVDF aerogels was measured using the transient plane source (TPS) technique in ambient conditions and at room temperature. The λ measured for the bulk PVDF pellet is around 0.18 W $m^{-1}K^{-1}$ and this value drastically reduces to 0.042 ± 0.003 W $m^{-1}K^{-1}$, 0.041 ± 0.003 W $m^{-1}K^{-1}$, and 0.040 ± 0.003 W $m^{-1}K^{-1}$ for α, β, and γ aerogels (~90% porosity), respectively. The solid conductivity of aerogels strongly depends on the density and the estimated densities for α, β, and γ aerogels are 0.14, 0.25, and 0.19 g cm^{-3}, respectively. These aerogels show exceptionally low λ values irrespective of the crystal structures, morphologies, and densities due to their multiscale porosities. These results suggest that thermal transport occurs majorly through the backbone of polymer chains. The gaseous conduction in aerogels is low because the gas molecules undergo collisions within the pores of the aerogels before their interactive scattering.[75, 76] It is worth mentioning here that the λ values of PVDF aerogels are comparable with other polymer aerogels.[6, 77-79]

After carefully examining the sound propagation characteristics, it is established that the pore structure and pore volume of a material have a significant influence on sound absorption. It means polymer aerogels not only exhibit thermal insulating characteristics but also show exceptional sound absorption capabilities, owing to their unique porous structures. As discussed in the preceding sections, α, β, and γ aerogels are lightweight, thermally stable, superhydrophobic, mechanically robust, and possess reasonably designed pore structures with a porosity of ~ 90%. As these aerogels qualify all the requirements of sound-insulating materials, their actual sound absorption coefficients (the ratio of absorbed sound intensity to the incident sound intensity) were further studied across different frequencies ranging from 0.2 to 6 kHz. The thickness of the cylindrical samples used for the measurements was kept around 12 mm. As illustrated in **Figure 7**, both α and β aerogels demonstrate impressive low-frequency absorption characteristics, boasting noise reduction coefficient (NRC) values of

0.41 and 0.43, respectively. The γ aerogel demonstrated exceptional sound absorption capabilities (NRC ~0.33), covering a broad frequency spectrum, beyond 1 kHz, and reaching its peak absorption coefficient of around ~1 within the frequency range of 1.5-3.5 kHz. These values are juxtaposed with those obtained for conventional commercial sound-insulating materials like expanded polystyrene (EPS), polyurethane (PU) foam, and expanded polyethylene (EPE), which are predominantly macroporous materials. Commercial sound-insulating materials and widely used fiber porous-based sound-absorbing materials show good medium and high-frequency noise-absorbing properties and they show poor absorption of low-frequency noise. The excellent low-frequency noise-absorbing properties of α, and β aerogels of PVDF can be attributed to their unique morphologies and highly mesoporous structures. When the sound waves incident, collision and friction dissipation occur within the meso and macroporous structures of these aerogels, and sound waves continuously reflect and dissipate in tortuous paths between the pores, and then the residual sound would be transmitted from the aerogels.[80, 81] The differences in the sound absorption capability in these α, β, and γ aerogels, particularly in low-frequency ranges (0.2 to 2.5 kHz), are mainly due to the difference in their pore structures and morphologies. The α form aerogel with nanofibrous network morphology engages the sound waves effectively, resulting in higher acoustic surface area and thus maximum dampening of lower frequency waves. On the other hand, the β and γ form aerogels with spherulite morphology provide rougher surfaces and create continuous impedance mismatches in their surroundings. PVDF aerogels present themselves as excellent alternatives to conventional acoustic insulators due to their exceptional sound absorption capabilities across a wide spectrum of frequencies especially providing better performance in the lower frequency range (0.2 to 2.5 kHz). These aerogels occasionally outperformed, currently available commercial sound insulation materials, particularly in specific frequency ranges. These aerogel structures are good for low-frequency noises

emanating from sources like road vehicles, aircraft, industrial machinery, artillery, and mining explosions.

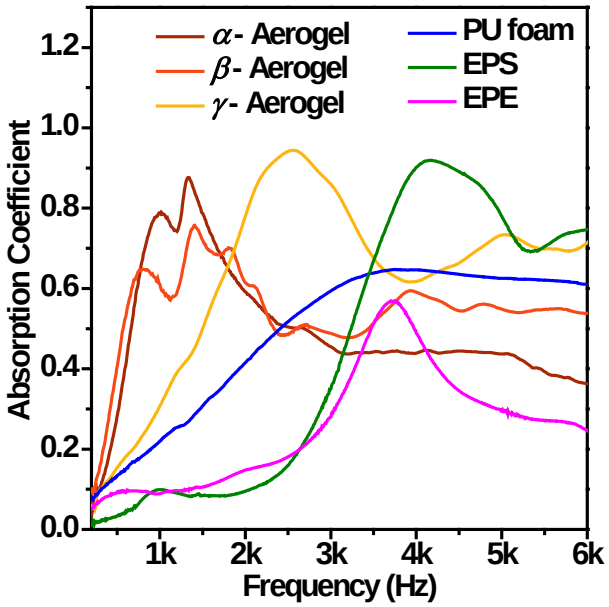

Figure 7. Normal incident sound absorption coefficients of α, β and γ aerogels along with commercially available sound insulation materials like EPS, PU foam, and EPE measured in the frequency range of 0.2 to 6 kHz.

Conclusions

In summary, we have successfully fabricated PVDF aerogels in their α, β, and γ crystalline forms through a precise selection of solvents, employing a straightforward and practical freeze-drying method. The initial gel solvents were replaced with environmentally friendly alternatives such as ethanol and water, which are suitable for a freeze-drying process to obtain aerogels. We achieved the α, β, and γ form aerogels, each with a porosity of ~90%, by carefully adjusting the initial PVDF loading. The successful isolation of each aerogel with a predominant fraction of a single polymorphic form was verified by WAXD and FTIR. It was found that polymer-solvent interactions play a significant role in the development of the structure and morphology of aerogels. The α form shows fibrillar morphology, while the β and γ forms show spherulitic morphology. The β form aerogel is mechanically more robust

compared to the α and γ form aerogels. The surface wettability of the aerogels revealed that the fabricated aerogels are superhydrophobic. The γ form displayed the highest WCA~151°, attributed to its unique morphology when compared to the α form (~132°) and the β form (~148°). The α and β form aerogels show excellent low-frequency sound absorption properties compared to the γ form due to their unique morphology differences. However, these aerogels showed almost the same thermal conductivity values (~0.040 ± 0.003 $Wm^{-1}K^{-1}$) irrespective of their morphologies. Further, the electroactive β form aerogel exhibited a higher remnant polarization (0.02 $\mu C/cm^2$) making it suitable for ferroelectric devices. The reported results indicate that the PVDF aerogels are suitable for multifunctional applications ranging from energy harvesting to thermal/acoustic insulation.

Associated Content:

Supporting Information:

Figures include WAXD plots, DSC thermograms, and Movie: Water droplet adhesion on the surface of the γ aerogel (Movie S1).

Author Information

Corresponding Author

*E-mail bhojegowd@niist.res.in; tel +91-471-2515474; fax +91-471-2491712 (E.B.G.).

laure.biniek@ics-cnrs.unistra.fr (L.B.).

ORCID

E. Bhoje Gowd: 0000-0002-2878-5845

Laure Biniek: 0000-0002-7643-3713

Conflict of Interest

The authors declare no competing financial interest.

Acknowledgments

EBG acknowledges the financial support from the Science & Engineering Research Board (SERB) (Research Project No. CRG/2021/002062) and the Council of Scientific and Industrial Research (CSIR), Government of India, New Delhi. T. N. and L.B. acknowledge ANR JCJC 2019 (BODYTEG: ANR-19- CE06-0004) for financial support. The authors acknowledge the financial support from CNRS International research program (IRP) entitled "Next-Generation (Macro)-Molecular Self-Assembled Systems (NEXTGEN)" for the visit of S.S. to ICS, Strasbourg. The authors acknowledge the technical support of Mr. R. B. Amal Raj. The authors also thank V. Harish Raj for the analytical assistance from CSIR-NIIST.

References

(1) Daniel, C.; Alfano, D.; Venditto, V.; Cardea, S.; Reverchon, E.; Larobina, D.; Mensitieri, G.; Guerra, G. Aerogels with a Microporous Crystalline Host Phase. *Adv. Mater.* **2005**, *17*, 1515-1518. DOI: 10.1002/adma.200401762.
(2) Daniel, C.; Giudice, S.; Guerra, G. Syndiotatic Polystyrene Aerogels with β, γ, and ε Crystalline Phases. *Chem. Mater.* **2009**, *21*, 1028-1034. DOI: 10.1021/cm802537g.
(3) Longo, S.; Vitillo, J. G.; Daniel, C.; Guerra, G. Monolithic Aerogels Based on Poly(2,6-Diphenyl-1,4-Phenylene Oxide) and Syndiotactic Polystyrene. *ACS Appl. Mater. Interfaces* **2013**, *5*, 5493-5499. DOI: 10.1021/am400592z.
(4) Krishnan, V. G.; Praveena, N. M.; Raj, R. B. A.; Mohan, K.; Gowd, E. B. Thermoreversible Gels of Poly(L-Lactide)/Poly(D-Lactide) Blends: A Facile Route to Prepare Blend α-Form and Stereocomplex Aerogels. *ACS Appl. Polym. Mater.* **2023**, *5*, 1556-1564. DOI: 10.1021/acsapm.2c02041.
(5) Liu, X.; Zhang, M.; Hou, Y.; Pan, Y.; Liu, C.; Shen, C. Hierarchically Superhydrophobic Stereo-Complex Poly (Lactic Acid) Aerogel for Daytime Radiative Cooling. *Adv. Funct. Mater.* **2022**, *32*, 2207414. DOI: 10.1002/adfm.202207414.
(6) Krishnan, V. G.; Joseph, A. M.; Kuzhichalil Peethambharan, S.; Gowd, E. B. Nanoporous Crystalline Aerogels of Syndiotactic Polystyrene: Polymorphism, Dielectric, Thermal, and Acoustic Properties. *Macromolecules* **2021**, *54*, 10605-10615. DOI: 10.1021/acs.macromol.1c01555.
(7) Joseph, A. M.; Nagendra, B.; Shaiju, P.; Surendran, K. P.; Gowd, E. B. Aerogels of Hierarchically Porous Syndiotactic Polystyrene with a Dielectric Constant near to Air. *J. Mater. Chem. C* **2018**, *6*, 360-368, DOI: 10.1039/C7TC05102F.
(8) D'Aniello, C.; Daniel, C.; Guerra, G. E Form Gels and Aerogels of Syndiotactic Polystyrene. *Macromolecules* **2015**, *48*, 1187-1193. DOI: 10.1021/ma502500n.
(9) Weinbach, Q.; Nielsen, C. B.; Biniek, L. Multi Length Scale Porosity as a Playground for Organic Thermoelectric Applications. *J. Mater. Chem. C* **2021**, *9*, 10173-10192, DOI: 10.1039/D1TC02331D.
(10) Berghams, H.; Donkers, A.; Frenay, L.; Stoks, W.; De Schryver, F. E.; Moldenaers, P.; Mewis, J. Thermoreversible Gelation of Syndiotactic Poly(Methyl Methacrylate). *Polymer* **1987**, *28*, 97-102. DOI: 10.1016/0032-3861(87)90322-3.
(11) Daniel, C.; Dammer, C.; Guenet, J.-M. On the Definition of Thermoreversible Gels: The Case of Syndiotactic Polystyrene. *Polymer* **1994**, *35*, 4243-4246. DOI: 10.1016/0032-3861(94)90604-1.

(12) Mal, S.; Maiti, P.; Nandi, A. K. On the Gelation Rates of Thermoreversible Poly(Vinylidene Fluoride) Gels. *Macromolecules* **1995**, *28*, 2371-2376. DOI: 10.1021/ma00111a034.
(13) Daniel, C.; Menelle, A.; Brulet, A.; Guenet, J.-M. Thermoreversible Gelation of Syndiotactic Polystyrene in Toluene and Chloroform. *Polymer* **1997**, *38*, 4193-4199. DOI: 10.1016/S0032-3861(96)01005-1.
(14) Dasgupta, D.; Nandi, A. K. Multiporous Polymeric Materials from Thermoreversible Poly(Vinylidene Fluoride) Gels. *Macromolecules* **2005**, *38*, 6504-6512. DOI: 10.1021/ma050601g.
(15) Talley, S. J.; Yuan, X.; Moore, R. B. Thermoreversible Gelation of Poly(Ether Ether Ketone). *ACS Macro Lett* **2017**, *6*, 262-266. DOI: 10.1021/acsmacrolett.7b00109.
(16) Dikshit, A. K.; Nandi, A. K. Thermoreversible Gelation of Poly(Vinylidene Flouride) in Diethyl Adipate: A Concerted Mechanism. *Macromolecules* **1998**, *31*, 8886-8892. DOI: 10.1021/ma980764n.
(17) Dikshit, A. K.; Nandi, A. K. Thermoreversible Gelation of Poly(Vinylidene Fluoride) in Diesters: Influence of Intermittent Length on Morphology and Thermodynamics of Gelation. *Macromolecules* **2000**, *33*, 2616-2625. DOI: 10.1021/ma990898g.
(18) Pierre, A. C.; Pajonk, G. M. Chemistry of Aerogels and Their Applications. *Chem. Rev.* **2002**, *102*, 4243-4266. DOI: 10.1021/cr0101306.
(19) Charlet, G.; Hong Phuong, N.; Delmas, G. Thermoreversible Gelation of Poly(4-Methyl-1-Pentene) in Cyclopentane and Cyclohexane. *Macromolecules* **1984**, *17*, 1200-1208. DOI: 10.1021/ma00136a017.
(20) Guenet, J. M. *Thermoreversible Gelation of Polymers and Biopolymers*; Academic Press, 1992.
(21) Cho, J. W.; Song, H. Y.; Kim, S. Y. Thermoreversible Gelation of Poly(Vinylidene Fluoride) in γ-Butyrolactone Solution. *Polymer* **1993**, *34*, 1024-1027. DOI: 10.1016/0032-3861(93)90224-X.
(22) Mandelkern, L. *Crystallization of Polymers: Volume 2, Kinetics and Mechanisms*; Cambridge University Press, 2004.
(23) Gowd, E. B.; Tashiro, K.; Ramesh, C. Structural Phase Transitions of Syndiotactic Polystyrene. *Prog. Polym. Sci.* **2009**, *34*, 280-315. DOI: 10.1016/j.progpolymsci.2008.11.002.
(24) Matsuda, H.; Inoue, T.; Okabe, M.; Ukaji, T. Study of Polyolefin Gel in Organic Solvents I. Structure of Isotactic Polypropylene Gel in Organic Solvents. *Polym. J.* **1987**, *19*, 323-329. DOI: 10.1295/polymj.19.323.
(25) Daniel, C.; Guerra, G.; Musto, P. Clathrate Phase in Syndiotactic Polystyrene Gels. *Macromolecules* **2002**, *35*, 2243-2251. DOI: 10.1021/ma011531q.
(26) Krishnan, V. G.; Joseph, A. M.; Kuzhichalil Peethambharan, S.; Gowd, E. B. Nanoporous Crystalline Aerogels of Syndiotactic Polystyrene: Polymorphism, Dielectric, Thermal, and Acoustic Properties. *Macromolecules* **2021**, *54*, 10605−10615. DOI: 10.1021/acs.macromol.1c01555.
(27) Matsuda, Y.; Fukatsu, A.; Wang, Y.; Miyamoto, K.; Mays, J. W.; Tasaka, S. Fabrication and Characterization of Poly(L-Lactic Acid) Gels Induced by Fibrous Complex Crystallization with Solvents. *Polymer* **2014**, *55*, 4369-4378. DOI: 10.1016/j.polymer.2014.06.086.
(28) Praveena, N. M.; Virat, G.; Krishnan, V. G.; Gowd, E. B. Stereocomplex Formation and Hierarchical Structural Changes During Heating of Supramolecular Gels Obtained by Polylactide Racemic Blends. *Polymer* **2022**, *241*, 124530. DOI: 10.1016/j.polymer.2022.124530.
(29) Talley, S. J.; Vivod, S. L.; Nguyen, B. A.; Meador, M. A. B.; Radulescu, A.; Moore, R. B. Hierarchical Morphology of Poly(Ether Ether Ketone) Aerogels. *ACS Appl. Mater. Interfaces* **2019**, *11*, 31508-31519. DOI: 10.1021/acsami.9b09699.
(30) Tazaki, M.; Wada, R.; Abe, M. O.; Homma, T. Crystallization and Gelation of Poly(Vinylidene Fluoride) in Organic Solvents. *J. Appl. Polym. Sci.* **1997**, *65*, 1517-1524. DOI: 10.1002/(SICI)1097-4628(19970822).
(31) Daniel, C.; Sannino, D.; Guerra, G. Syndiotactic Polystyrene Aerogels: Adsorption in Amorphous Pores and Absorption in Crystalline Nanocavities. *Chem. Mater.* **2008**, *20*, 577-582. DOI: 10.1021/cm702475a.

(32) Figueroa-Gerstenmaier, S.; Daniel, C.; Milano, G.; Vitillo, J. G.; Zavorotynska, O.; Spoto, G.; Guerra, G. Hydrogen Adsorption by δ and ε Crystalline Phases of Syndiotactic Polystyrene Aerogels. *Macromolecules* **2010**, *43*, 8594-8601. DOI: 10.1021/ma101218q.
(33) Daniel, C.; Pellegrino, M.; Venditto, V.; Aurucci, S.; Guerra, G. Nanoporous-Crystalline Poly(2,6-Dimethyl-1,4-Phenylene)Oxide (PPO) Aerogels. *Polymer* **2016**, *105*, 96-103. DOI: 10.1016/j.polymer.2016.10.017.
(34) Cui, Z.; Hassankiadeh, N. T.; Zhuang, Y.; Drioli, E.; Lee, Y. M. Crystalline Polymorphism in Poly(Vinylidenefluoride) Membranes. *Prog. Polym. Sci.* **2015**, *51*, 94-126. DOI: 10.1016/j.progpolymsci.2015.07.007.
(35) Martins, P.; Lopes, A. C.; Lanceros-Mendez, S. Electroactive Phases of Poly(Vinylidene Fluoride): Determination, Processing and Applications. *Prog. Polym. Sci.* **2014**, *39*, 683-706. DOI: 10.1016/j.progpolymsci.2013.07.006.
(36) Lovinger, A. J. Recent Developments in the Structure, Properties, and Applications of Ferroelectric Polymers. *Jpn. J. Appl. Phys.* **1985**, *24*, 18. DOI: 10.7567/JJAPS.24S2.18.
(37) Takahashi, Y.; Matsubara, Y.; Tadokoro, H. Crystal Structure of Form II of Poly(Vinylidene Fluoride). *Macromolecules* **1983**, *16*, 1588-1592. DOI: 10.1021/ma00244a007.
(38) Davies, G. R.; Singh, H. Evidence for a New Crystal Phase in Conventionally Poled Samples of Poly(Vinylidene Fluoride) in Crystal Form II. *Polymer* **1979**, *20*, 772-774. DOI: 10.1016/0032-3861(79)90253-2.
(39) Weinhold, S.; Litt, M. H.; Lando, J. B. The Crystal Structure of the γ Phase of Poly(Vinylidene Fluoride). *Macromolecules* **1980**, *13*, 1178-1183. DOI: 10.1021/ma60077a029.
(40) Lovinger, A. J. Ferroelectric Polymers. *Science* **1983**, *220*, 1115-1121. DOI: 10.1126/science.220.4602.1115.
(41) Hasegawa, R.; Takahashi, Y.; Chatani, Y.; Tadokoro, H. Crystal Structures of Three Crystalline Forms of Poly(Vinylidene Fluoride). *Polym. J.* **1972**, *3*, 600-610. DOI: 10.1295/polymj.3.600.
(42) Tashiro, K.; Yamamoto, H.; Kummara, S.; Takahama, T.; Aoyama, K.; Sekiguchi, H.; Iwamoto, H. High-Electric-Field-Induced Hierarchical Structure Change of Poly(Vinylidene Fluoride) as Studied by the Simultaneous Time-Resolved WAXD/SAXS/FTIR Measurements and Computer Simulations. *Macromolecules* **2021**, *54*, 2334-2352. DOI: 10.1021/acs.macromol.0c02567.
(43) Tashiro, K.; Yamamoto, H.; Kummara, S.; Tahara, D.; Aoyama, K.; Sekiguchi, H. Electric-Field-Induced Phase Transition and Crystal Structural Change of the Oriented Poly(Vinylidene Fluoride) β Form as Clarified by the in Situ Synchrotron Wide-Angle X-Ray Diffraction Measurement. *Macromolecules* **2022**, *55*, 6644-6660. DOI: 10.1021/acs.macromol.2c01015.
(44) Bachmann, M. A.; Lando, J. B. A Reexamination of the Crystal Structure of Phase II of Poly(Vinylidene Fluoride). *Macromolecules* **1981**, *14*, 40-46. DOI: 10.1021/ma50002a006.
(45) Lando, J. B.; Olf, H. G.; Peterlin, A. Nuclear Magnetic Resonance and X-Ray Determination of the Structure of Poly(Vinylidene Fluoride). *J. Polym. Sci., Part A: Polym. Chem.* **1966**, *4*, 941-951. DOI: 10.1002/pol.1966.150040420.
(46) Banik, N. C.; Boyle, F. P.; Sluckin, T. J.; Taylor, P. L.; Tripathy, S. K.; Hopfinger, A. J. Theory of Structural Phase Transitions in Poly(Vinylidene Fluoride). *Phys. Rev. Lett.* **1979**, *43*, 456-460. DOI: 10.1103/PhysRevLett.43.456.
(47) Takahashi, Y.; Tadokoro, H. Crystal Structure of Form III of Poly(Vinylidene Fluoride). *Macromolecules* **1980**, *13*, 1317-1318. DOI: 10.1021/ma60077a057.
(48) Kang, S. J.; Bae, I.; Choi, J.-H.; Park, Y. J.; Jo, P. S.; Kim, Y.; Kim, K. J.; Myoung, J.-M.; Kim, E.; Park, C. Fabrication of Micropatterned Ferroelectric Gamma Poly(Vinylidene Fluoride) Film for Non-Volatile Polymer Memory. *J. Mater. Chem.* **2011**, *21*, 3619-3624, DOI: 10.1039/C0JM02732D.
(49) Davis, G. T.; McKinney, J. E.; Broadhurst, M. G.; Roth, S. C. Electric-Field-Induced Phase Changes in Poly(Vinylidene Fluoride). *J. Appl. Phys.* **2008**, *49*, 4998-5002. DOI: 10.1063/1.324446.
(50) Li, M.; Wondergem, H. J.; Spijkman, M.-J.; Asadi, K.; Katsouras, I.; Blom, P. W. M.; de Leeuw, D. M. Revisiting the δ-Phase of Poly(Vinylidene Fluoride) for Solution-Processed Ferroelectric Thin Films. *Nat. Mater.* **2013**, *12*, 433-438. DOI: 10.1038/nmat3577.

(51) Naegele, D.; Yoon, D. Y.; Broadhurst, M. G. Formation of a New Crystal Form (α_p) of Poly(Vinylidene Fluoride) under Electric Field. *Macromolecules* **1978**, *11*, 1297-1298. DOI: 10.1021/ma60066a051.
(52) Bachmann, M.; Gordon, W. L.; Weinhold, S.; Lando, J. B. The Crystal Structure of Phase IV of Poly(Vinylidene Fluoride). *J. Appl. Phys.* **2008**, *51*, 5095-5099. DOI: 10.1063/1.327425.
(53) Dasgupta, D.; Malik, S.; Thierry, A.; Guenet, J. M.; Nandi, A. K. Thermodynamics, Morphology, and Structure of the Poly(Vinylidene Fluoride)−Ethyl Acetoacetate System. *Macromolecules* **2006**, *39*, 6110-6114. DOI: 10.1021/ma0610921.
(54) Dasgupta, D.; Manna, S.; Garai, A.; Dawn, A.; Rochas, C.; Guenet, J. M.; Nandi, A. K. Morphology, Structure, Rheology, and Thermodynamics of Piezoelectric Poly(Vinylidene Fluoride)−Ethylene Carbonate Thermoreversible Gel. *Macromolecules* **2008**, *41*, 779-787. DOI: 10.1021/ma7021502.
(55) Yadav, P. J. P.; Aswal, V. K.; Sastry, P. U.; Patra, A. K.; Maiti, P. Thermoreversible Gelation of Poly(Vinylidene Fluoride-Co-Hexafluoro Propylene) in Phthalates. *J. Phys. Chem. B* **2009**, *113*, 13516-13525. DOI: 10.1021/jp907047b.
(56) Yadav, P. J. P.; Maiti, B.; Ghorai, B. K.; Sastry, P. U.; Patra, A. K.; Aswal, V. K.; Maiti, P. Thermoreversible Gelation of Poly(Vinylidene Fluoride-Co-Chlorotrifluoroethylene): Structure, Morphology, Thermodynamics, and Theoretical Prediction. *Macromolecules* **2011**, *44*, 3029-3038. DOI: 10.1021/ma200271j.
(57) Wang, M.; Liu, W.; Shi, X.; Pan, J.; Zhou, B.; Wang, J.; Sun, T.; Tang, Y. Highly Efficient and Continuous Triboelectric Power Harvesting Based on a Porous B-Phase Poly(Vinylidene Fluoride) Aerogel. *New J. Chem.* **2021**, *45*, 1893-1898, DOI: 10.1039/D0NJ05134A.
(58) Yu, S.; Zhang, Y.; Yu, Z.; Zheng, J.; Wang, Y.; Zhou, H. PANI/PVDF-TrFE Porous Aerogel Bulk Piezoelectric and Triboelectric Hybrid Nanogenerator Based on in-Situ Doping and Liquid Nitrogen Quenching. *Nano Energy* **2021**, *80*, 105519. DOI: 10.1016/j.nanoen.2020.105519.
(59) Zhang, J.; Kong, Y.; Shen, X. Polyvinylidene Fluoride Aerogel with High Thermal Stability and Low Thermal Conductivity. *Mater. Lett.* **2020**, *259*, 126890. DOI: 10.1016/j.matlet.2019.126890.
(60) Torres-Rodriguez, J.; E. Bedolla, D.; D'Amico, F.; Koopmann, A.-K.; Vaccari, L.; Saccomano, G.; Kohns, R.; Huesing, N. Polyvinylidene Fluoride Aerogels with Tailorable Crystalline Phase Composition. *Gels* **2022**, *8*, 727.
(61) Suresh, S.; Krishnan, V. G.; Dasgupta, D.; Surendran, K. P.; Gowd, E. B. Directional-Freezing-Enabled Mxene Orientation toward Anisotropic PVDF/MXene Aerogels: Orientation-Dependent Properties of Hybrid Aerogels. *ACS Appl. Mater. Interfaces* **2023**, *15*, 49567-49582. DOI: 10.1021/acsami.3c09845.
(62) Weinbach, Q.; Thakkar, S. V.; Carvalho, A.; Chaplais, G.; Combet, J.; Constantin, D.; Stein, N.; Collin, D.; Biniek, L. Efficient Control of a Mesoporous Fibrillar PEDOT:PSS Aerogel Structure for Promising Thermoelectric Applications. *Front. Electron. Mater* **2022**, *2*, 875856. DOI: 10.3389/femat.2022.875856.
(63) K. Tashiro, Crystal Structure and Phase Transition of PVDF and Related Copolymers, H. S. Nalwa, Ed., Ferroelectric Polymers: Chemistry, Physics and Applications, Marcel Dekker, New York, **1995**, 63-182.
(64) Gaßdorf, F.; Fan, Z.; Schwaderer, J.; Beuermann, S.; Wilhelm, R.; Weber, A. P.; Fischlschweiger, M. Macromolecular Architecture-Dependent Polymorphous Crystallization Behavior of PVDF in the PVDF/γ-BL System Via Thermally Induced Phase Separation. *Macromol. Rapid Commun.* **2023**, *44*, 2300177. DOI: 10.1002/marc.202300177.
(65) Aubert, J. H. Isotactic Polystyrene Phase Diagrams and Physical Gelation. *Macromolecules* **1988**, *21*, 3468-3473. DOI: 10.1021/ma00190a021.
(66) Cai, X.; Lei, T.; Sun, D.; Lin, L. A Critical Analysis of the α, β and γ Phases in Poly(Vinylidene Fluoride) Using FTIR. *RSC Adv.* **2017**, *7*, 15382-15389, DOI: 10.1039/C7RA01267E.
(67) Okabe, M.; Wada, R.; Tazaki, M.; Homma, T. The Flory-Huggins Interaction Parameter and Thermoreversible Gelation of Poly(Vinylidene Fluoride) in Organic Solvents. *Polym. J.* **2003**, *35*, 798-803. DOI: 10.1295/polymj.35.798.

(68) Yeow, M. L.; Liu, Y. T.; Li, K. Isothermal Phase Diagrams and Phase-Inversion Behavior of Poly(Vinylidene Fluoride)/Solvents/Additives/Water Systems. *J. Appl. Polym. Sci.* **2003**, *90*, 2150-2155. DOI: 10.1002/app.12846.
(69) Tashiro, K.; Kobayashi, M.; Tadokoro, H. Vibrational Spectra and Disorder-Order Transition of Poly(Vinylidene Fluoride) Form III. *Macromolecules* **1981**, *14*, 1757-1764. DOI: 10.1021/ma50007a028.
(70) Rajak, A.; Rühe, J. High Hysteresis Suspended Wetting State: A Wetting Regime for Controlled Trapping of Drops on Micro-Trench Covered Surfaces. *Adv. Mater. Interfaces* **2022**, *9*, 2201018. DOI: 10.1002/admi.202201018.
(71) Cassie, A. B. D.; Baxter, S. Wettability of Porous Surfaces. *Trans. Faraday Soc.* **1944**, *40*, 546-551, DOI: 10.1039/TF9444000546.
(72) Rosenberg, Y.; Siegmann, A.; Narkis, M.; Shkolnik, S. The Sol/Gel Contribution to the Behavior of γ-Irradiated Poly(Vinylidene Fluoride). *J. Appl. Polym. Sci.* **1991**, *43*, 535-541. DOI: 10.1002/app.1991.070430314.
(73) Furukawa, T.; Johnson, G. E. Measurements of Ferroelectric Switching Characteristics in Polyvinylidene Fluoride. *Appl. Phys. Lett.* **1981**, *38*, 1027-1029. DOI: 10.1063/1.92232.
(74) Takahashi, T.; Date, M.; Fukada, E. Dielectric Hysteresis and Rotation of Dipoles in Polyvinylidene Fluoride. *Appl. Phys. Lett.* **2008**, *37*, 791-793. DOI: 10.1063/1.92076.
(75) Li, M.; Qin, Z.; Cui, Y.; Yang, C.; Deng, C.; Wang, Y.; Kang, J. S.; Xia, H.; Hu, Y. Ultralight and Flexible Monolithic Polymer Aerogel with Extraordinary Thermal Insulation by a Facile Ambient Process. *Adv. Mater. Interfaces* **2019**, *6*, 1900314. DOI: 10.1002/admi.201900314.
(76) Samitsu, S. Thermally Stable Mesoporous Poly(Ether Sulfone) Monoliths with Nanofiber Network Structures. *Macromolecules* **2018**, *51*, 151-160. DOI: 10.1021/acs.macromol.7b02217.
(77) Fan, J.; Ifuku, S.; Wang, M.; Uetani, K.; Liang, H.; Yu, H.; Song, Y.; Li, X.; Qi, J.; Zheng, Y.; et al. Robust Nanofibrillated Cellulose Hydro/Aerogels from Benign Solution/Solvent Exchange Treatment. *ACS Sustainable Chemistry & Engineering* **2018**, *6*, 6624-6634. DOI: 10.1021/acssuschemeng.8b00418.
(78) Mıhlayanlar, E.; Dilmaç, Ş.; Güner, A. Analysis of the Effect of Production Process Parameters and Density of Expanded Polystyrene Insulation Boards on Mechanical Properties and Thermal Conductivity. *Mater. Des.* **2008**, *29*, 344-352. DOI: 10.1016/j.matdes.2007.01.032.
(79) Fan, W.; Zhang, X.; Zhang, Y.; Zhang, Y.; Liu, T. Lightweight, Strong, and Super-Thermal Insulating Polyimide Composite Aerogels under High Temperature. *Compos. Sci. Technol.* **2019**, *173*, 47-52. DOI: 10.1016/j.compscitech.2019.01.025.
(80) He, C.; Huang, J.; Li, S.; Meng, K.; Zhang, L.; Chen, Z.; Lai, Y. Mechanically Resistant and Sustainable Cellulose-Based Composite Aerogels with Excellent Flame Retardant, Sound-Absorption, and Superantiwetting Ability for Advanced Engineering Materials. *ACS Sustain. Chem. Eng.* **2018**, *6*, 927-936. DOI: 10.1021/acssuschemeng.7b03281.
(81) Oh, J.-H.; Kim, J.; Lee, H.; Kang, Y.; Oh, I.-K. Directionally Antagonistic Graphene Oxide-Polyurethane Hybrid Aerogel as a Sound Absorber. *ACS Appl. Mater. Interfaces* **2018**, *10*, 22650-22660. DOI: 10.1021/acsami.8b06361.

ToC

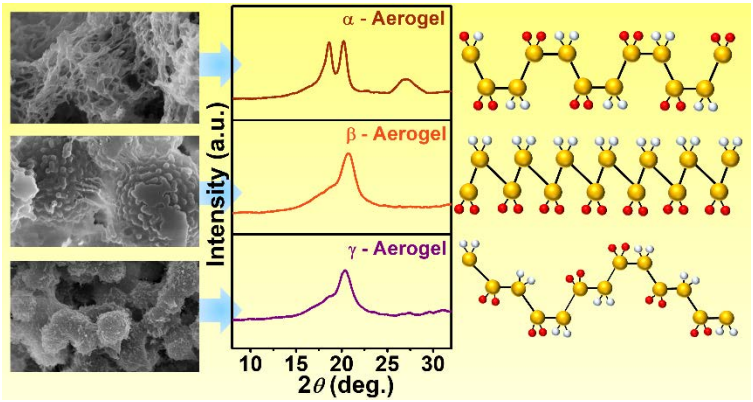
α - Aerogel
β - Aerogel
γ - Aerogel
Intensity (a.u.)
10 15 20 25 30
2θ (deg.)